

Scaling relationship for oscillating electrochemical systems: dependence of phase diagram on electrode size and rotation rate

István Z. Kiss,^a Zoltán Kazsu^b and Vilmos Gáspár^{*b}

Received 17th March 2009, Accepted 22nd May 2009

First published as an Advance Article on the web 19th June 2009

DOI: 10.1039/b905295j

Dynamics of oscillations in electrochemical systems are affected by both *chemical* and *physical* properties of the systems. Chemical properties include the type of electrochemical reaction, the electrode material, the composition of the electrolyte, *etc.*, while physical properties include the solution resistance, the cell constant, the electrode size, the rotation rate, the external resistance, *etc.* Earlier, we proposed the application of cell-geometry-independent phase-diagrams to characterize the oscillatory regions in the electrode potential *vs.* external resistance parameter plane. In this report, we investigate how this type of phase diagram changes with the surface area (electrode radius) and the rotation rate of an electrode. Based on linear stability analysis of a general, two-variable model for negative-differential resistance (NDR) type electrochemical oscillators we propose a scaling relationship. It predicts that all scaled data points derived from the critical values of parameters (resistance and potential) characterizing the onset of oscillations should fall—independently of the size of the electrode and the rotation rate—on a single plot. The analytical predictions are tested in both numerical simulations and experiments with copper electrodisolution in phosphoric acid.

1. Introduction

Electrochemical systems exhibit a wide range of oscillatory behaviour including smooth or relaxation type periodic, quasi-periodic, and chaotic waveforms.^{1–4} The dynamical behaviour depends not only on the surface concentration of electrochemically active species but also on the potential drop across the double-layer. It has been noted that when the electrode potential plays an essential role in the origin of current oscillations, the electrochemical system exhibits (at least hidden) negative differential resistance (NDR) in a certain region of the overpotential. Chemical reactions that can produce negative differential resistance include metal passivation, potential dependent adsorption of an inhibitor, desorption of a catalyst and reactions exhibiting Frumkin-effects or chemical autocatalysis.²

However, the presence of NDR is only a necessary, but not sufficient condition for current oscillations. The occurrence of oscillations in an electrochemical cell is affected not only by the chemical properties of the system (the type of electrochemical reaction, the electrode material, the composition of the electrolyte, *etc.*) but also by several physical effects related to the rate of mass transfer (*e.g.*, the rotation rate of a rotating disk electrode, the electrolyte viscosity) or to the potential drop in the solution or in the external circuitry (*e.g.*, solution

resistance, cell constant, electrode size, external resistance, *etc.*).^{1–4} Whether an electrochemical system is oscillatory or not strongly depends on the physical parameters of the electrochemical cell. Many of the observations indicated that a minimal uncompensated potential (IR) drop is required: current oscillations were observed on large electrodes³ and at large rotation rates.^{5–7} The minimal IR drop was experimentally measured for iron electrodisolution for different sulfuric acid concentrations and rotation rates.⁸ These observations are expected to hold for a large class of electrochemical systems, because the underlying mechanisms (presence of NDR with sufficient external IR drop) are common features of electrochemical oscillations. We have proposed a non-traditional phase diagram with the use of impedance spectroscopy: the oscillatory regions were mapped in the electrode potential *vs.* external resistance parameter plane⁹ and thus were independent of the presence of IR drop in the cell.

In this paper, we determine the quantitative dependence of the oscillatory regions of NDR systems on two important experimental parameters: the electrode surface area A (or electrode radius r) and rotation rate d . Based on linear stability analysis of a general, two-variable model for NDR-type electrochemical oscillators an analytical relationship is proposed for the A and d dependence of the non-traditional phase diagrams. The analytical approximations are tested in both numerical simulations and experiments with copper electrodisolution in phosphoric acid. Finally, the significance and limitations of the obtained results are discussed concerning the predictability of oscillatory regions in electrochemical systems.

^a Department of Chemistry, Saint Louis University, 3501 Laclede Avenue, St. Louis, MO 63103, USA. E-mail: izkiss@slu.edu; Fax: +1 314 977 2521; Tel: +1 314 977 2139

^b Institute of Physical Chemistry, University of Debrecen, 4032 Debrecen, Egyetem tér 1, Hungary. E-mail: gasparv@delfin.unideb.hu; Fax: +36 52 512 915; Tel: +36 52 512 900 ext. 22389

2. Analytical prediction: a scaling relationship for NDR-type electrochemical oscillators

A general, two variable model of a potentiostatic NDR type electrochemical oscillator¹⁰ is given by the following set of ordinary differential equations:

$$C_d \frac{de}{dt} = \frac{V - e}{AR_s} - nFk(e)c \quad (1)$$

$$\frac{dc}{dt} = -\frac{2}{a}k(e)c + \frac{2D_o}{a^2}(c_o - c) \quad (2)$$

Eqn (1) and (2) describe the charge and mass balance, respectively, for an electrochemical process. The dynamical variables are the electrode potential e and the near-surface concentration of the electroactive species c . C_d is the double layer capacitance, A is the surface area of the electrode, V is the circuit potential, R_s is series resistance (including solution resistance), F is the Faraday constant, n is the number of electrons in the reduction reaction, a is the Nernst diffusion layer thickness, D_o and c_o are the diffusion constant and the bulk concentration of the electroactive species, respectively. $k(e)$ is the potential dependent rate constant; for NDR systems considered in this study $k(e)$ exhibits N-shaped dependence on e with a negative differential resistance region.²

In a typical potentiostatic experiment the current $i(t) = (V - e(t))/R_s$ is measured while the circuit potential V is kept constant. The dynamical behavior of the equations has been analyzed in great detail.^{2,4} It was shown that oscillation can develop if $dk(e)/de < 0$, i.e., when there is negative slope on the polarization curve (N-NDR system).

At the steady state (e_{ss} , c_{ss}) the limiting current density j_l is defined as

$$j_l = \frac{V - e_{ss}}{AR_s} = nFk(e_{ss})c_{ss} \quad (3)$$

Based on eqn (2), its value can be calculated as follows:

$$j_l = \frac{nFD_o}{a}(c_o - c_{ss}) \quad (4)$$

By considering that in the mass transfer region $c_{ss} \approx 0$, and taking into account the known relationship between the thickness (a) of the Nernst diffusion layer and the rotation rate (d) of the electrode¹¹

$$a = \frac{\beta}{d^{0.5}} \quad (5)$$

where β is a constant, one arrives at the Levich equation:¹¹

$$j_l = \frac{nFD_o c_o}{\beta} d^{0.5} \quad (6)$$

Linear stability analysis (see the Appendix) predicts that the locus of Hopf points (onset of oscillations through Hopf bifurcations) varies with rotation rate d as follows

$$R_H A = C(e_{ss}) + \frac{D(e_{ss})}{d^{0.5}} \quad (7)$$

where R_H is the solution resistance at the Hopf point,

$$C(e_{ss}) = -\frac{1}{nFc_o \frac{dk(e_{ss})}{de}} \quad (8)$$

and

$$D(e_{ss}) = -\frac{k(e_{ss})\beta}{nFc_o D_o \frac{dk(e_{ss})}{de}} \quad (9)$$

Note that in these equations both C and D depend on the electrode potential at the bifurcation point. The relationship defined by eqn (7) can be interpreted qualitatively with the assumption that there is a minimal $IR = \text{constant}$ potential drop, which is required to induce oscillations.⁸ According to the Levich equation¹¹ the current will be proportional to $d^{0.5}$ (see eqn (6)). Therefore, the critical resistance at which oscillations are expected to occur should scale with $1/d^{0.5}$. By rearranging eqn (7), one can predict a similar but somewhat more complicated dependence: the $R_H A$ value minus a potential dependent constant (C) will be inversely proportional to the square root of the rotation rate as follows:

$$R_H A - C(e_{ss}) = \frac{D(e_{ss})}{d^{0.5}} \quad (10)$$

This scaling relationship has been tested experimentally during the anodic electrodisolution of a rotating copper disk electrode in phosphoric acid electrolyte and numerically by using the three variable Koper–Gaspard model of this system.

3. Experimental

Experiments were performed by using a standard three-electrode electrochemical cell equipped with a copper rotating disk electrode (RDE), a saturated calomel electrode (Radelkis OH-0933P) as reference, and a Pt-sheet counter electrode (Radelkis OH-9437, area 5 cm²). A computer controlled potentiostat (Elektroflex EF451) was applied to set the potential (resolution 0.01 mV) between the working and reference electrodes. All potentials are given with respect to the SCE. The current was measured with an ammeter (accuracy 0.001 mA) built in the potentiostat. The sampling frequency for data acquisition was 200 Hz. The cell was thermostated at 20 ± 0.1 °C. Orthophosphoric acid (Merck or Reanal, 85%) was used as received. A small cut of a copper rod (3, 5, and 7 mm diameter) was fixed in the Teflon holder of a Tacussel RDE apparatus that allowed the variation of rotation rate with an accuracy of 1 rpm. The surface of the copper electrode (99.99% purity) was freshly polished by a series of wet sanding treatments. To remove the oxide layer from the surface of the copper electrode, the potential was first set to 500 mV for 2 min then swept in several cycles between 0 and 750 mV with a scan rate of 10 mV s⁻¹. Next the series (ohmic) resistance R_s of the solution was determined from impedance measurements in the frequency range of 5–10 kHz at 100 ± 20 mV rest potential. The value of R_s was determined by averaging the results of three independent measurements: linear extrapolation of the impedance spectrum to infinite frequency where the imaginary part of the total impedance is zero.

4. Model equations

The Koper–Gaspard dimensionless model¹² is applied to simulate anodic electrodisolution of a rotating copper disk electrode in phosphoric acid electrolyte

$$\frac{de}{dt} = \frac{V - e}{R_s A} - mk(e)u \quad (11)$$

$$\frac{du}{dt} = -\frac{5}{4}d^{1/2}k(e)u + 2d(w - u) \quad (12)$$

$$\frac{dw}{dt} = \frac{8}{5}d(2 - 3w + u) \quad (13)$$

where V is the applied circuit potential, e is the electrode potential, R_s is the serial resistance, A is the electrode surface area, d is the rotation rate, u and w are the concentrations of some electroactive species, respectively, in the surface- and diffusion-layers. The potential dependent rate constant $k(e)$ is defined as:

$$k(e) = 2.5\theta^2 + 0.01 \exp[0.5(e - 30)] \quad (14)$$

where θ is related to the potential dependent surface coverage by the electroactive species:

$$\theta = \begin{cases} 1 & \text{for } e \leq 35 \\ \exp[-0.5(e - 35)^2] & \text{for } e > 35 \end{cases} \quad (15)$$

The experimentally measured quantity, the current, is obtained as $i = (V - e)/R_s$. Dynamics of model eqn (11)–(13) have been studied in detail by Koper and Gaspard.¹² For an appropriate range of parameters ($m = 120$, $d = 0.1$ – 0.2 , $R_s A = 0.01$ – 0.05) the model simulates well the dynamical behaviour of Cu electrodisolution in phosphoric acid observed in our experiments.^{9,13} In this study, the dynamical features are further explored by systematically varying the electrode size and rotation rate.

5. Results and discussion

5.1 Numerical simulations

Numerical integration of eqn (11)–(13) at $d = 0.14$ and $R_s A = 0.02$ results in an onset of oscillations at $V = 36.659$. The corresponding (mean) electrode potential is $e = 35.803$. The $R_s A$ value corresponding to the given rotation rate and electrode potential could also be approximated using the scaling relationship (eqn (7)–(9)). Note that the relationship has been derived from the general two variable model of an NDR type electrochemical oscillator (eqn (1)–(2)). However, the main sources of (simple) periodic dynamics both in the two variable skeleton model and the three variable Koper–Gaspard model¹² are the same: the presence of NDR in the polarization curve and the slow diffusion of the electroactive species from the solution bulk to the electrode surface. The third variable w in the Koper–Gaspard model was introduced in order to account for the experimentally observed mixed-mode and chaotic oscillations. We note that w is a slow dynamical variable in the model and, therefore, it is non-essential for simple periodic oscillations. Consequently, by

setting dw/dt to zero in eqn (13), it is possible to eliminate w as a variable. The resulting two dimensional system is dynamically equivalent to the general skeleton model (eqn (1)–(2)). By formally applying the scaling relationship to this reduced 2D system for the conditions given above we obtain:

$$C(e_{ss}) = -\frac{1}{m\left(\frac{dk(e)}{de}\right)_{ss}} = 4.134 \times 10^{-3} \quad (16)$$

and

$$D(e_{ss}) = -\frac{15}{16} \frac{k(e_{ss})}{m\left(\frac{dk(e)}{de}\right)_{ss}} = 5.789 \times 10^{-3} \quad (17)$$

Based on these values, the scaling relationship (eqn (7)) predicts $R_H A = 0.0196$ for $d = 0.14$. This approximated value is only 2.0% less than the exact value used in the numerical integrations (0.02). They are not identical because of the approximations in obtaining equation A5 from A4 and of some small effects of w .

These results imply that (i) the analytical predictions based on the skeleton model are transferable to a more realistic 3D model and (ii) the approximation of neglecting the second term on the right hand side of equation A4 is justified for the oscillatory condition.

The dependence of Hopf bifurcation points on the circuit potential (V) and cell resistance ($R_s A$) are often shown in ‘traditional’ phase diagrams where the oscillatory regions are depicted in V vs. $R_s A$ plane.^{2,4} In our earlier study,⁹ we proposed a non-traditional phase diagram in which the (inverse) resistance at which Hopf bifurcations occur are plotted as a function of the electrode potential at which the bifurcations appear (Hopf potentials). This non-traditional phase diagram offers the advantage of separating IR drop effects from kinetic effects on the oscillatory dynamics. For model eqn (11)–(13), the locus of Hopf bifurcations points in the non-traditional phase space was determined by a two-parameter (V and $R_s A$) branch following continuation method using the AUTO interface of XPPAUT.¹⁴ The obtained bell shape curve at $d = 0.1$ is shown in Fig. 1. Based on the curve one can predict the oscillatory region at any $R_s A$ value:⁹ the intersections of a horizontal lines $1/(R_s A)$ with the bell-shape locus define the Hopf bifurcation points of the system. That is, the relative position of the $1/R_s A$ lines and the locus of Hopf bifurcations determine the region of oscillations. Thus the effects of electrode radius and rotation rate on the region of oscillations can be described by the effect of these parameters on the $1/R_s A$ line and the Hopf curve.

Effect of electrode radius. The non-traditional phase diagram (electrode potential vs. $1/R_H A$) is independent of the presence of IR drop in the cell. Note that the surface area (electrode radius) appears only in the first term of the right hand side of eqn (1) that defines the IR drop. Therefore, one can foresee that the change of the electrode radius does not change the position of the bell shaped Hopf curve in the phase diagram.

However, changing the surface area (the electrode radius) will change the $R_s A$ value and thus the position of the $1/R_s A$

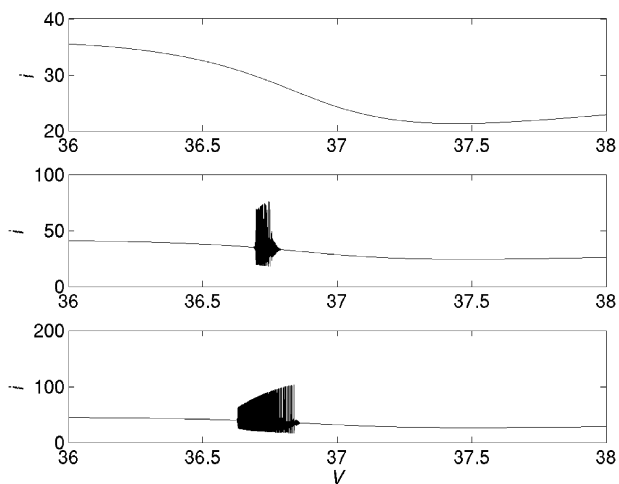
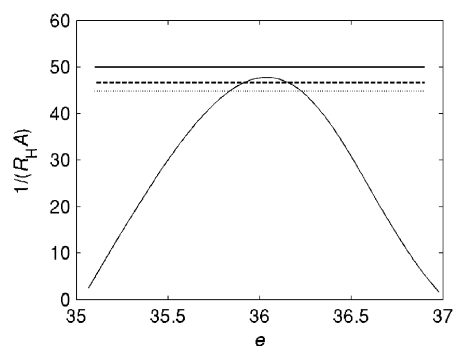


Fig. 1 Simulation: effect of electrode radius on current oscillations. Top figure: locus of Hopf bifurcation points at $d = 0.1$. For a given electrode $R_s A = 0.03545r$. The intersections of the horizontal line $1/(R_s A)$ and the Hopf curve give the oscillatory range in the electrode potential e . At $r = 0.63$ (dotted) and $r = 0.605$ (dashed) oscillations are expected, while at $r = 0.564$ (solid) oscillations are not possible. Bottom figure: anodic polarization scans with $v_{\text{scan}} = 0.001$, $d = 0.1$, $R_s A = 0.03545r$ and $r = 0.564$ (top), 0.605 (middle), and 0.63 (bottom).

line. For a disk electrode¹⁵ $R_s A = r\pi/4\kappa$, where κ is the specific conductivity of the electrolyte. Therefore, $R_s A$ linearly varies with radius r . Consequently, at sufficiently small electrode the $1/R_s A$ line can be pushed above the maximum of the bell shaped curve, and the oscillations can be eliminated. Since there is a minimal electrode radius above which oscillations can develop, current oscillations could be induced by increasing the size of the electrode.

The effect of radius on the oscillatory region is illustrated in Fig. 1 for $d = 0.1$. For our model calculations, we assume that $R_s A = 0.03545r$; this hypothetical dependence reflects the linear dependence of $R_s A$ on electrode radius. For relatively small electrode, $r = 0.564$, the $1/R_s A$ line (solid line in Fig. 1) does not have intersection with the Hopf curve. Therefore, oscillations do not occur in the polarization scans (see top scans in Fig. 1). In contrast, at $r = 0.605$ the $1/R_s A$ (dashed) line crosses the Hopf curve and thus a small oscillatory region is observed in the (middle) polarization scan. For $r = 0.63$, the $1/R_s A$ (dotted) line gives two well separated intersections with the Hopf curve, therefore, the (bottom) polarization scan produces a relatively wide oscillatory region.

The appearance of current oscillations at the bifurcation points are shown in the polarization scan is consistent with prediction of the phase diagram and implies the existence of oscillations above a minimal electrode radius. Note that the bell shape curve ends for large values of $R_H A$. Therefore, in accordance with the theory of electrochemical oscillations^{2,4} there is also a maximum electrode radius above which current oscillations cannot be found.

Effect of rotation rate. The effect of the rotation rate on the oscillatory region is different from that of the electrode radius. The rotation rate will not affect the $R_s A$ values and thus the position of the $1/R_s A$ line; instead it affects the Hopf curve as it was shown by the linear stability analysis (see eqn (7)). The location of Hopf points varies with the rotation rate d such that the bell shaped curve moves upward as d is increased. Therefore, at a fixed electrode size there is a minimum rotation rate above which oscillation can occur.

Fig. 2 shows the effect of rotation rate on the dynamics of the model system. The bell shaped locus moves upward as the

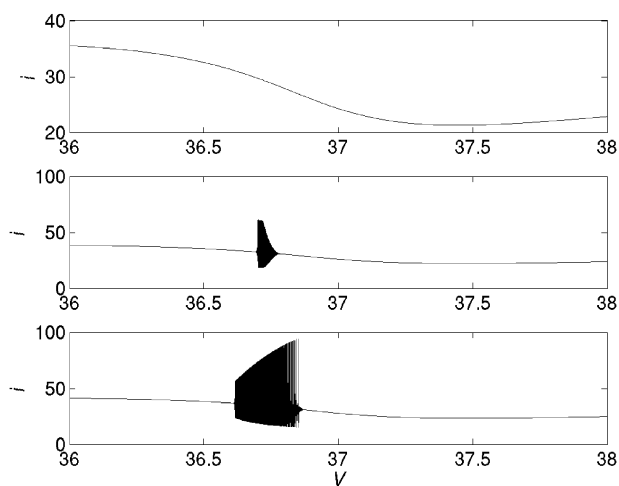
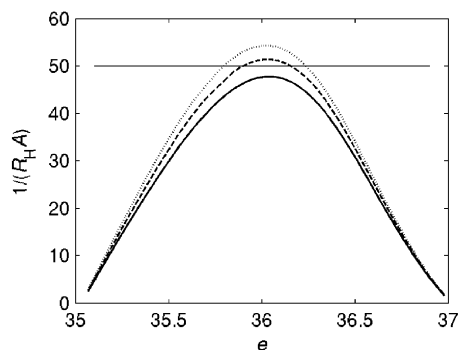


Fig. 2 Simulation: effect of rotation rate on current oscillations. Top figure: locus of Hopf bifurcation points at three representative rotation rates $d = 0.14$ (top, dotted), 0.12 (middle, dashed), and 0.1 (bottom, solid). For the electrode radius $r = 0.564$ ($R_s A = 0.02$) the intersections of the horizontal line $1/(R_s A)$ and the Hopf curves give the oscillatory range in the electrode potential e . For $d = 0.14$ and 0.12 oscillations are expected, while for $d = 0.1$ oscillations are not possible. Bottom figure: anodic polarization scans with $v_{\text{scan}} = 0.001$, at electrode radius $r = 0.564$ and $d = 0.1$ (top), $d = 0.12$ (middle) and $d = 0.14$ (bottom).

value of rotation rate d is increased. For the electrode radius $r = 0.564$ ($R_s A = 0.02$) the intersections of the horizontal line $1/(R_s A)$ and the Hopf curves give the oscillatory range in the electrode potential e . For $d = 0.14$ and 0.12 oscillations are expected, while for $d = 0.1$ oscillations are not possible. In the polarization scans (see Fig. 2) there are no oscillations for $d = 0.1$; there is a narrow and wide oscillatory region for $d = 0.12$ and 0.14 , respectively. These polarization scans are in agreement with the prediction based on the changes in the position of the Hopf curve in the phase diagram at various rotation rates.

Eqn (7) also predicts that at a given electrode potential the $R_H A$ values corresponding to the Hopf points are inversely proportional to the square-root of the rotation rate. Fig. 3 shows the calculated series of loci as the rotation rate d is varied between 0.1 and 1.0 with 0.1 increments from which the critical $1/R_H A$ values corresponding to a given electrode potential e can be determined. The series of $R_H A$ vs. $d^{-0.5}$ type plots (bottom Fig. 3) at different electrode potential values confirm the predicted scaling relationship.

Eqn (10) predicts that all scaled data points derived from the critical values of parameters (resistance and potential) characterizing the onset of current oscillations should fall—independently of the size of the electrode and the rotation rate—on the diagonal of $(R_H A - C)$ vs. $D/d^{0.5}$ coordinate system. We determined the C (e_{ss}) and D (e_{ss}) values by linear least square fit of data points in Fig. 3 according to eqn (10). Fig. 4 shows that the general scaling relationship holds for all data points in the simulations.

5.2 Experiments

Effect of electrode radius. The locus of Hopf bifurcation points in the experimental system has been obtained by impedance spectroscopy (see ref. 9 for details) using disk

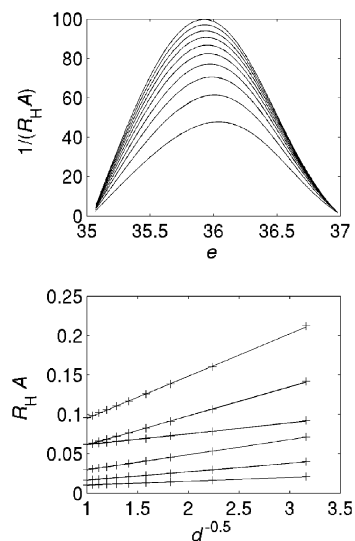


Fig. 3 Simulation: effect of rotation rate on the phase diagram. Top figure: locus of Hopf bifurcation points at different rotation rates d varying between 0.1 and 1.0 with 0.1 increments from the bottom curve to top one. Bottom figure: $R_H A$ vs. $d^{-0.5}$ curves from bottom to top in the order of $e = 35.1, 35.13, 35.24, 35.41, 36.1, \text{ and } 36.8$ confirming the scaling relationship.

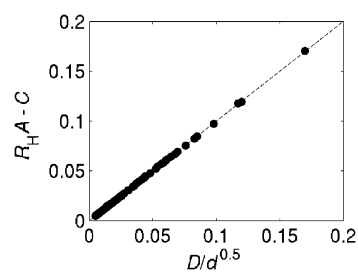


Fig. 4 Simulation: scaling relationship $(R_H A - C)$ vs. $D/d^{0.5}$ for all the data shown in Fig. 3.

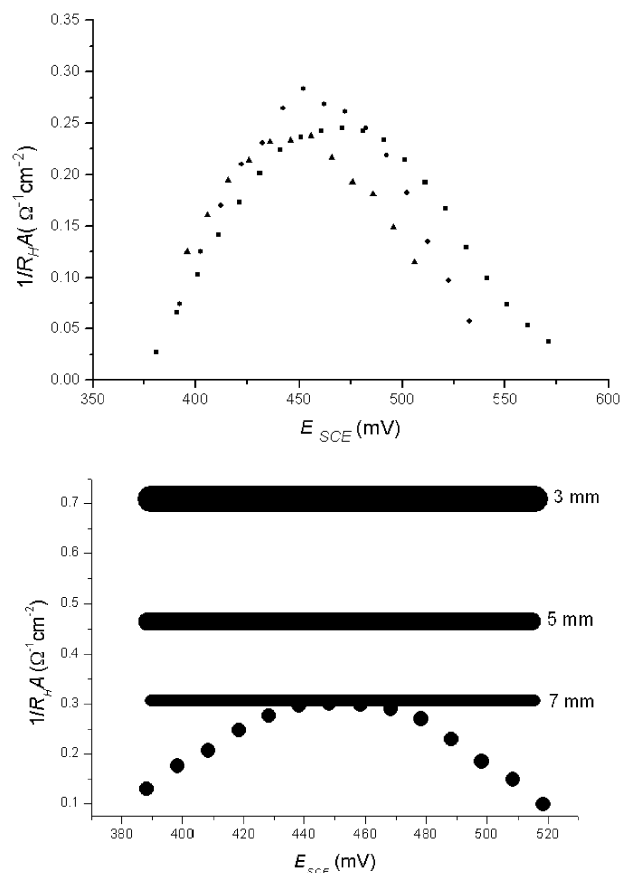


Fig. 5 Experiments: top figure: scaled locus of Hopf bifurcation points in the experimental system obtained by impedance spectroscopy at rotation rate 1000 min^{-1} (see ref. 9 for details). The diameter of the electrodes are 3 (\blacktriangle), 5 (\bullet) and 7 (\blacksquare) mm. Bottom figure: Scaled locus of Hopf bifurcation points in the experimental system measured with 3-mm electrode at rotation rate 1500 min^{-1} . The horizontal bars show the $1/(R_s A)$ values for electrodes of different sizes (determined with impedance spectroscopy); the thickness of the bar indicates error values in determining R_s values. Only the 7 mm electrode is expected to oscillate.

electrodes of 3, 5 and 7 mm diameter. Fig. 5 shows that regardless of the electrode radius very similar bell shaped curves apply to each electrode at a rotation rate 1000 min^{-1} . Although the surface area has been increased by a factor of 5.44 the peak of the locus of bifurcation points are reproduced within *ca.* 20% in the $1/R_H A$ quantities. The curves are also quite well reproduced in the horizontal (*i.e.*, electrode

potential) direction within 25 mV. In other words, similar to the calculations, the scaled locus can be considered invariant to the size of the electrode. The series resistance was determined for each electrode (3, 5 and 7 mm diameter) with impedance spectroscopy; none of the $1/R_s A$ lines would intersect the bell shaped curves, therefore, no oscillation is expected to occur at rotation rate of 1000 rpm.

In the bottom figure the scaled locus is shown at rotation rate 1500 min^{-1} and measured with an electrode of 3 mm diameter. The horizontal bars give the $1/(R_s A)$ values for the applied electrodes; the thickness of the bar indicates the error values in determining R_s with impedance spectroscopy. Based on the experimental data, only the 7 mm electrode intersects the bell shaped curve and thus only this largest electrode is expected to show current oscillations.

Fig. 6 shows polarization scans of the 5 and 7 mm diameter electrodes at different rotation rates. As it is expected from the phase diagrams in Fig. 5, a scan of a rotating copper disk electrode of 5 mm diameter does not exhibit oscillations (top figure of Fig. 5). (We note that oscillations were not observed with the 3 mm diameter electrode either.) In contrast, the 7 mm diameter electrode does exhibit oscillations at the larger, 1500 min^{-1} rotation rate without any attached external resistance as shown in the bottom figure of Fig. 6. These results indicate that the phase diagrams in Fig. 5 can predict

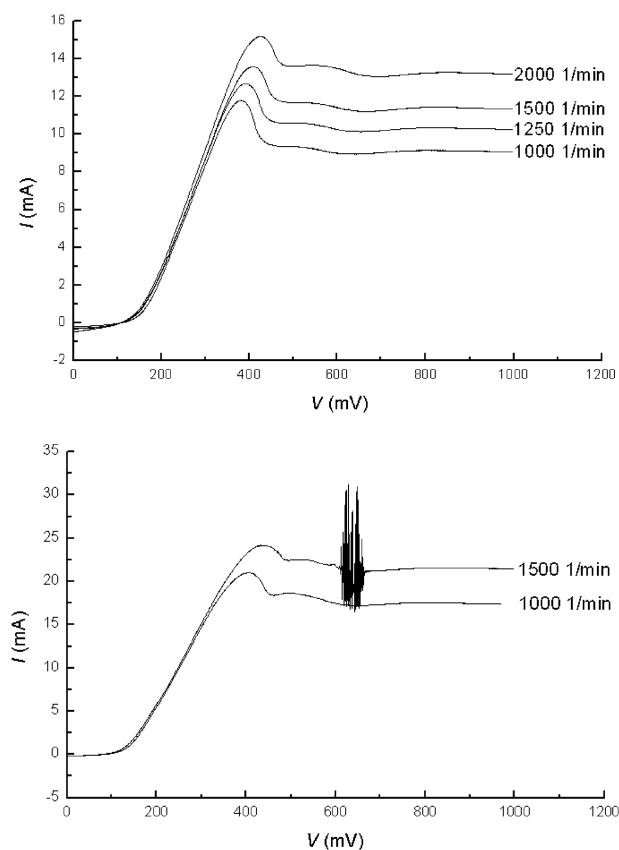


Fig. 6 Experiments: top figure: anodic polarization scans of a rotating copper disk electrode of 5 mm diameter at different rotation rates. Scan rate: 10 mV s^{-1} . Bottom figure: anodic polarization scans of a rotating copper disk electrode of 7 mm diameter at different rotation rates. Scan rate: 10 mV s^{-1} .

the diameter of the electrode at which spontaneous current oscillation can be observed without attaching an external resistance to the cell. Because the electrode diameter only affects the position of $1/(R_s A)$ lines, there will be a minimum electrode diameter above which current oscillations can be observed.

Effect of rotation rate. The effect of rotation rate on the oscillatory region can be interpreted both qualitatively and quantitatively using the results of the linear stability analysis summarized in eqn (7).

Qualitatively, we expect that, by increasing the rotation rate, the locus of Hopf bifurcation points shift to upwards direction at each Hopf potential; because the position of the $1/R_s A$ line does not change it is expected that a small enough electrode that does not exhibit oscillations can show transitions to oscillations at larger rotation rates. This qualitative effect is well reproduced in Fig. 6 where the 7 mm diameter electrode starts to exhibit oscillations at a rotation rate of 1500 rpm. We conclude that the experiments qualitatively confirm the predicted effect of rotation rate: current oscillations are induced through shifting the bell curve in the upward direction.

In order to quantitatively test the validity of the scaling relation eqn (7), the locus of Hopf bifurcation points has been determined in a large range of rotation rates with an electrode of 3 mm diameter. The series of curves is shown in the top figure of Fig. 7. As expected from eqn (7), the bell shaped curve is being moved upward as the rotation rate is increased. Plots of $R_H A$ vs. $d^{-0.5}$ curves created at various electrode potentials from the top series of the scaled locus of Hopf points are shown in the middle and bottom figures. In these plots a linear variation is expected to occur with C and D values changing with the potential. The experimentally obtained linear trend in these Figures indicate that the scaling relationship eqn (7) holds well in a large potential region of 285 mV–380 mV; the scaling relationship is difficult to evaluate in a 20 mV range at the beginning (265 mV–285 mV) and the end (380 mV–400 mV) of the potential region where the locus of bifurcation points of different rotation rates starts to overlap.

Similar to the numerical simulations, the scaled data points again fall on the diagonal of $(R_H A - C)$ vs. $D/d^{0.5}$ coordinate system (Fig. 8). This finding also shows that the critical resistance at which oscillations occur in case of NDR-type electrochemical oscillators is inversely proportional to the square root of the rotation rate. We consider this scaling relationship as a type of dynamical Levich equation¹¹ for electrochemical oscillators.

6. Conclusions

Traditional non-equilibrium phase diagrams¹⁶ map systems' behaviour in a (typically two-dimensional) parameter space. Such phase diagrams have been proven to be useful tools to characterize the qualitative behaviour (*e.g.*, number of steady states, types of oscillations and patterns) of nonlinear systems.

In electrochemical systems two important parameters that set the dynamics and thus characterize the onset of current oscillations are the series cell resistance and the applied

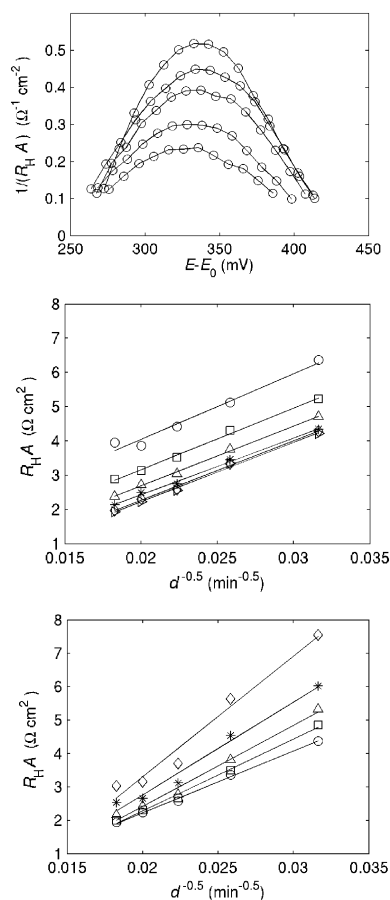


Fig. 7 Experiments: top figure: locus of Hopf bifurcation points from top to bottom at rotation rates 3000, 2500, 2000, 1500 and 1000 min^{-1} . The diameter of the electrode is 3 mm. Middle and bottom figures confirm the scaling relation in the experiments at various electrode potentials. The scaling relationship holds at all potentials. $E - E_0$ (mV) in the middle figure: \circ 285, \square 295, \triangle 305, $*$ 315, \diamond 325, \triangleright 335, and in the bottom figure: \circ 340, \square 350, \triangle 360, $*$ 370, \diamond 380 where E_0 is the equilibrium potential.

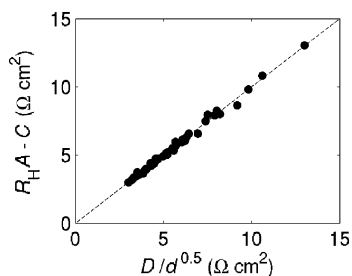


Fig. 8 Experiments: scaling relationship $(R_{\text{H}A} - C)$ vs. $D/d^{0.5}$ for all the data shown in Fig. 7.

external potential. Potential vs. resistance type phase diagrams are useful for a specific electrochemical cell,^{2,4} however, they strongly depend on the cell geometry (*e.g.*, relative position of working, reference, and counter electrodes, size of the electrodes) of the cell. A non-traditional phase diagram⁹ for the oscillatory regions can be constructed by replacing the circuit potential with the corresponding electrode potential. The two quantities differ by the potential drop in the electrolyte and the external

circuitry. Because the external IR drop is subtracted from the applied potential, the obtained phase diagrams do not depend on the cell resistance. Moreover, the non-traditional phase diagrams provide a convenient way of studying the effects of physical parameters on the dynamics of electrochemical oscillators.

The phase diagram (when the resistance is given per surface area) does not depend on the surface area of the working electrode. We showed in numerical simulations and experiments with NDR electrochemical oscillators, that in this case, the effect of surface area can be interpreted by a change of the cell resistance. In the phase diagram, the increase of the electrode potential region for oscillatory dynamics with increasing the surface area is contributed to the decreased $1/R_{\text{s}}A$ values. We note that by increasing the electrode size to a large extent, the oscillations could become strongly non-uniform by changing the synchronization characteristics of the oscillations or by spatial bifurcations resulting in oscillations with complicated spatial characteristics.² However, the focus of our approach is on the prediction of the onset uniform oscillations and thus spatial effects are discarded.

The phase diagram strongly depends on the rotation rate of the electrode. Since electrochemical oscillations are induced by a minimal IR drop^{2,8} and the limiting current has a Levich-type square-root dependence on the rotation rate,¹¹ it is quite reasonable that the resistance at which oscillations arise scales with the inverse square root of the rotation rate. Therefore, the derived scaling relationship (eqn (7)) can be considered as a dynamical Levich-type equation for oscillatory electrochemical systems.

In contrast to the effect of the electrode size, the increased potential region for the oscillation with increasing the rotation rate can be interpreted by the upward shift of the bell-shaped curve of the locus of Hopf bifurcations in the phase diagram while the cell resistance remains constant. The limitations of the obtained relationship are similar to those of the Levich equation including laminar flow around the electrode,¹¹ at very large rotation rates turbulent flow, at very low rotation rates the appearance of diffusive mass transport would complicate the description. We note, however, that many NDR oscillators require mass transport that diffusion cannot provide¹ and thus the laminar, well-defined flow of the rotating electrode is a common way of studying electrochemical oscillations.

The obtained relationships considering the external resistance, surface area and rotation rate imply that the phase diagrams measured at a certain parameter sets can be transformed to other parameters. Such a transformation thus can be applied to either search for electrochemical oscillations, or, alternatively, to map the conditions for stable cell operation. The phase diagrams are constructed with impedance measurements under stable conditions; if such conditions are not found IR compensation can be used along with the impedance measurements.

The phase diagrams could also provide a way for studying the effects of other experimental parameters, *e.g.*, temperature. Our studies show that by changes of temperature the oscillatory region is not greatly affected in the Cu phosphoric acid system. The increase of cell resistance due to temperature

decrease to 273 K is compensated by a downward shift of the phase diagrams; the two effects are similar in magnitude and thus the oscillatory regions do not change significantly. The presented phase diagrams could be useful tools for the investigations of the non-trivial temperature effects on oscillations, for example, temperature compensation or inverse temperature effects.¹⁷

Our analysis is based on the investigation of NDR electrochemical oscillators with supercritical Hopf bifurcations. However, electrochemical systems can also exhibit subcritical Hopf bifurcations¹⁸ or homoclinic bifurcations.¹⁹ With subcritical bifurcations the oscillatory region is often underestimated since the oscillatory boundary in this case is often marked by the saddle-node bifurcation of periodic orbits that accompany subcritical Hopf bifurcations in low-dimensional nonlinear systems.¹⁶ An NDR oscillator with hidden negative resistance can exhibit saddle-loop bifurcation;¹⁹ in this case the oscillatory region is overestimated by the Hopf bifurcation points since the stable limit cycle is destroyed in a homoclinic bifurcation. In both examples, however, our analysis would give an indication of the possible occurrence of oscillations in the predicted parameter regions.

Appendix

The locus of Hopf points as a function of rotation rate d at constant double-layer potential e can be predicted by linear stability analysis. The Jacobian matrix of the general two variable model for NDR type electrochemical oscillators defined by eqn (1) and (2) is as follows:

$$\mathbf{J} = \begin{pmatrix} -\frac{1}{C_d R_H A} - \frac{n F c_{ss} \frac{dk(e)}{de}}{C_d} & -\frac{n F k(e)}{C_d} \\ -\frac{2c \frac{dk(e)}{de}}{a} & -\frac{2k(e)}{a} - \frac{2D_o}{a^2} \end{pmatrix} \quad (\text{A1})$$

At the Hopf bifurcation point ($e = e_{ss}$, $c = c_{ss}$), where $R_s = R_H$, $\text{Tr } \mathbf{J} = 0$, that is

$$-\frac{1}{C_d R_H A} - \frac{n F c_{ss} \frac{dk(e_{ss})}{de}}{C_d} - \frac{2k(e_{ss})}{a} - \frac{2D_o}{a^2} = 0 \quad (\text{A2})$$

It follows from eqn (2) that at the steady state (e_{ss} , c_{ss})

$$-\frac{2}{a} k(e_{ss}) - \frac{2D_o}{a^2} = -\frac{2D_o}{a^2} \frac{c_o}{c_{ss}} \quad (\text{A3})$$

Substituting eqn (A3) into (A2) results in the following condition for the Hopf bifurcation:

$$\frac{1}{R_H A} = -n F c_{ss} \frac{dk(e_{ss})}{de} - \frac{2D_o C_d c_o}{a^2 c_{ss}} \quad (\text{A4})$$

Our numerical simulations indicated that the first term on the right hand side of eqn (A4) is the major contributing term to the positive $1/R_H A$ value in the oscillatory NDR region where $dk(e_{ss})/de < 0$. The second, negative term typically decreases the $1/R_H A$ value by about 2%. (See section 5.1 for a specific example.)

Assuming that the first term of the above equation is much greater than the second one, eqn (A4) is simplified to eqn (A5).

$$\frac{1}{R_H A} = -n F c_{ss} \frac{dk(e_{ss})}{de} \quad (\text{A5})$$

From eqn (2), the value of c_{ss} is as follows

$$c_{ss} = \frac{c_o}{k(e_{ss}) \frac{a}{D_o} + 1} \quad (\text{A6})$$

Therefore, the locus of Hopf points can be given by eqn (A7):

$$\frac{1}{R_H A} = \frac{-n F c_o \frac{dk(e_{ss})}{de}}{1 + \frac{k(e_{ss})a}{D_o}} \quad (\text{A7})$$

Taking into account the relationship between the thickness (a) of the diffusion layer and the rotation rate (d) as defined by eqn (5) leads to the following scaling relation

$$R_H A = -\frac{1}{n F c_o \frac{dk(e_{ss})}{de}} - \frac{k(e_{ss})\beta}{n F c_o D_o \frac{dk(e_{ss})}{de}} \frac{1}{d^{0.5}} \quad (\text{A8})$$

Applying the following definitions

$$C(e_{ss}) = -\frac{1}{n F c_o \frac{dk(e_{ss})}{de}} \quad (\text{A9})$$

and

$$D(e_{ss}) = -\frac{k(e_{ss})\beta}{n F c_o D_o \frac{dk(e_{ss})}{de}} \quad (\text{A10})$$

we arrive at eqn (A11) (eqn (7) in the text) that will be tested numerically and experimentally:

$$R_H A = C(e_{ss}) + \frac{D(e_{ss})}{d^{0.5}} \quad (\text{A11})$$

The other necessary condition for a Hopf bifurcation to occur is that $\text{Det } \mathbf{J} > 0$. For the general, two variable model system (eqn (1) and (2)) the determinant is as follows

$$\text{Det } \mathbf{J} = \frac{2 \left(k(e_{ss})a + D_o + R_H A D_o n F c_{ss} \frac{dk(e_{ss})}{de} \right)}{C_d R_H A a^2} \quad (\text{A12})$$

By taking into account that at the Hopf point $\text{Tr } \mathbf{J} = 0$, and substituting the resulting expression for the derivative from (A2) into (A12), we obtain a simplified formula for the determinant that does not contain the derivative of the rate constant:

$$\text{Det } \mathbf{J} = \frac{2k(e_{ss})}{C_d R_H A a} - \frac{4k(e_{ss})D_o}{a^3} - \frac{4D_o^2}{a^4} \quad (\text{A13})$$

For an oscillatory system at the bifurcation point eqn (A13) should be positive with $1/R_H A$ defined in eqn (A4). These conditions cannot be satisfied for arbitrary value of rotation rate d ; therefore, the scaling relationship (eqn (A9)–(11)) shall be observed only for a range of rotation rates. General analysis of this range is difficult, however it is easy to show that oscillations are not possible for very low and very high rotation rates. At high rotation rates when $d \rightarrow \infty$, $a \rightarrow 0$, and $R_H A \rightarrow C$, the value of $\text{Det } \mathbf{J}$ goes to negative in eqn (A13). It means that at infinite large rotation rate there are no oscillations. At low rotation rates when $d \rightarrow 0$, $a \rightarrow \infty$, and $c_{ss} \rightarrow 0$, the $1/R_H A$ values will become negative in equation A4. However, negative $1/R_H A$ values will always produce negative $\text{Det } \mathbf{J}$ in eqn (A13) and thus oscillations are again not possible.

Based on this simple argument, it is expected that the scaling relationship (eqn (A9)–(11)) can be applied within a certain range of rotation rates where simple periodic oscillations occur through Hopf bifurcation; this range has been determined numerically in the Koper–Gaspard model.¹²

Acknowledgements

V. G. thanks OTKA T60417 for financial support.

References

- 1 J. L. Hudson and T. T. Tsotsis, *Chem. Eng. Sci.*, 1994, **49**, 1493–1572.
- 2 K. Krischer, in *Modern Aspects of Electrochemistry*, ed. B. E. Conway, O. M. Bockris and R. E. White, Kluwer Academic/Plenum Press, New York, 1999, vol. 32, p. 1.
- 3 S. Glarum and J. H. Marshall, *J. Electrochem. Soc.*, 1985, **132**, 2872–2878.
- 4 M. T. M. Koper, *Adv. Chem. Phys.*, 1996, **92**, 161–298.
- 5 F. N. Albahadily, J. Ringland and M. Schell, *J. Chem. Phys.*, 1989, **90**, 813–821.
- 6 F. N. Albahadily and M. Schell, *J. Chem. Phys.*, 1988, **88**, 4312–4319.
- 7 M. Schell and F. N. Albahadily, *J. Chem. Phys.*, 1989, **90**, 822–828.
- 8 D. Sazou and M. Pagitsas, *Electrochim. Acta*, 2006, **51**, 6281–6296.
- 9 I. Z. Kiss, V. Gáspár and L. Nyikos, *J. Phys. Chem. A*, 1998, **102**, 909–914.
- 10 M. T. M. Koper and J. H. Sluyters, *J. Electroanal. Chem.*, 1991, **303**, 73–94.
- 11 E. Gileadi, *Electrode Kinetics for Chemists, Chemical Engineers and Material Scientists*, VCH, New York, 1993.
- 12 M. T. M. Koper and P. Gaspard, *J. Chem. Phys.*, 1992, **96**, 7797–7813.
- 13 I. Z. Kiss, V. Gáspár, L. Nyikos and P. Parmananda, *J. Phys. Chem. A*, 1997, **101**, 8668–8674.
- 14 B. Ermentrout, *Simulating, Analyzing and Animating Dynamical Systems: A Guide to XPPAUT for Researchers and Students*, SIAM, Philadelphia, 2002.
- 15 J. Newman and K. E. Thomas-Alyea, *Electrochemical Systems*, Wiley, 2004.
- 16 I. R. Epstein and J. A. Pojman, *An Introduction to Nonlinear Chemical Dynamics: Oscillations, Waves, Patterns, and Chaos*, Oxford University Press, Oxford, 1998.
- 17 R. Nagao, I. R. Epstein, E. R. Gonzalez and H. Varela, *J. Phys. Chem. A*, 2008, **112**, 4617–4624.
- 18 A. Karantonis, Y. Shiomi and S. Nakabayashi, *Int. J. Bifurcation Chaos*, 2001, **11**, 1275–1294.
- 19 D. Haim, O. Lev, L. M. Pismen and M. Sheintuch, *J. Phys. Chem.*, 1992, **96**, 2676–2681.